

Contents lists available at ScienceDirect

Journal of Alloys and Compounds

journal homepage: www.elsevier.com/locate/jalcom





Effects of Ni content on microstructure and fracture toughness of the ZrN/TiNiN nano-multilayer films

Jingjing Wang ^{a,1}, Yingyun Cai ^{a,1}, Wei Li ^{a,*}, Ping Liu ^a, Xun Ma ^a, Ke Zhang ^a, Fengcang Ma ^a, Xiaohong Chen ^a, Peter K. Liaw ^b

ARTICLE INFO

Keywords: ZrN/TiNiN nano-multilayer films Magnetron sputtering Microstructure Coherent epitaxy Fracture toughness

ABSTRACT

ZrN and TiNiN nanolayers are alternately deposited on silicon substrate by magnetron sputtering. A series of ZrN/TiNiN nano-multilayer films with different Ni contents are prepared by varying the Ni:Ti volume ratio of the targets. The effects of Ni content on the microstructures and mechanical properties of ZrN/TiNiN nano-multilayer films are studied by X-ray diffractometer (XRD), scanning electron microscopy (SEM), high resolution transmission electron microscopy (HRTEM) and nanoindentation instrument. The results show that with the increase of Ni content, the crystallization degree of ZrN phase first increases and then decreases. Besides, the hardness, elastic modulus and toughness of the films also increase first and then decrease with Ni content increasing. When Ni:Ti= 1:24, the ZrN/TiNiN nano-multilayer films obtain the highest hardness, elastic modulus and fracture toughness, which are 23.2 GPa, 317.8 GPa and 2.29 MPa·m¹/², respectively. This is mainly attributed to the best columnar crystal growth of the ZrN/TiNiN nano-multilayer film. The TiNiN layer changes into face centered cubic structure under the template of ZrN layer, and grows in coherent epitaxy with ZrN layer.

1. Introduction

In recent years, with the rapid development of modern science and technology, the requirements for the materials used in the fields of biology, environment and national defense have become increasingly demanding [1–4]. Among those materials, the nano-multilayer films as a typical representative have been widely concerned. On the one hand, nano-multilayer films materials can play the synergistic advantages of the component materials [5,6]. On the other hand, the interfacial effect between the two monolayer interfaces, which impedes the movement of dislocations, can have a reinforcing effect [7]. Therefore, the nano-multilayer films can significantly exhibit good comprehensive mechanical properties [8,9], such as the improved plasticity and toughness on the basis of satisfying the strength, which have good development and application prospects in the fields of aerospace, machining, and biology [10–18]. As a typical hard multilayer, transition metal nitride (TMN) nano-multilayer has a broad application in engineering field because of its high hardness, good thermal stability and high melting point [19-22]. However, in practical engineering

applications, the hardness and toughness of TMN nano-multilayer films hardly be met at the same time, which greatly restricts the application and development of TMN nano-multilayer films in the field of advanced manufacturing. Therefore, the development of TMN nano-multilayer films with the integrative properties of strength and toughness is of great significance to expand their engineering applications.

In recent years, there are two main toughening mechanisms of hard nano-multilayer films, namely, phase structure transformation in the modulated layer and the coherent/non-coherent interface [23]. Among them, the phase transformation toughening of the separated phase in the sublayer is considered as a promising method to improve the toughness of hard nano-multilayer films [24]. Wang et al. [25] prepared $Fe_{82}Mn_{18}/TiB_2$ and $Fe_{65}Mn_{35}/TiB_2$ nano-multilayer films by magnetron sputtering and realized phase transformation toughening. It was account to volume expansion of the crystal structure through the stress of the component phase in the modulating layer. In the TiN-Ni nanocomposite films [26], separation of the TiN and Ni phases was observed. Also, the crystallinity of the Ni phase and an increase in TiN and Ni crystallite sizes had great effects on the mechanical properties, such as hardness,

E-mail address: liwei176@usst.edu.cn (W. Li).

^a School of Materials and Chemistry, University of Shanghai for Science and Technology, Shanghai 200093, PR China

^b Department of Materials Science and Engineering, The University of Tennessee, Knoxville, TN 37996, USA

^{*} Corresponding author.

¹ These authors contributed equally to this work

ductile and intrinsic stress. Besides, the TiN-Ni nanocomposite film was achieved a 3-fold increase in the critical load for crack formation, while maintaining a hardness higher than 25 GPa, which was correlated with the intrinsic properties of the nanostructure. In addition, it was found that by increasing the Ni concentration from 5 at% to 30%, the metal Ni particles were encapsulated by the TiN network structure, achieving a maximum hardness of approximately 28 GPa [27]. Therefore, the TiNiN layer can be used as the modulation layer of nano-multilayer film for phase separation, thus tailoring the integrative properties of strength and toughness by varying the Ni content.

ZrN has high hardness, good wear resistance and fatigue properties. Therein, its high hardness makes the film resistant to crack sprouting and expansion very poorly, which seriously limits the practical applications under the complex and demanding conditions [28-31]. However, when ZrN acts as a layer in the nano-multilayer films, its microstructure and properties such as resistance to crack growth, namely, fracture toughness, will be greatly improved [32-37]. For example, a maximum fracture resistance was achieved in the ZrN/ZrAlN nano-multilayer films when the modulation layer ZrAlN thickness was 2 nm [34]. It is because the ZrAlN layer and ZrN layer maintained the epitaxially growth, and the phase separation of ZrN-rich and cubic-phase AlN occurred in the ZrAlN layer. Also, the transformation of cubic-structured AlN to wurtzite-structured AlN resulted in volume expansion and residual compressive stresses, leading to significant toughening effects. Besides, the similar phenomenon was also observed in the ZrN/AlTiN nano-multilayer films [35]. The hexagonal close packed (hcp) structure of AlN was transformed into face-centered cubic (FCC) structure and ZrN structure was epitaxially grown on the (111) crystal plane, making the films exhibiting good fracture toughness. Therefore, it is concluded that ZrN as one of the layers of nano-multilayer films will play an important role in improving the mechanical properties.

In this paper, ZrN and TiNiN are alternately deposited using magnetron sputtering technique, thus constituting ZrN/TiNiN nanomultilayer films, where ZrN is the main layer and TiNiN is the modulation layer. Therein, a series of ZrN/TiNiN nano-multilayer films by varying the Ni content in the TiNiN modulation layer are obtained to investigate the microstructures, mechanical properties, as well as fracture toughness. The hardening and toughening mechanisms of the ZrN/TiNiN nano-multilayer films are clarified.

2. Experimental details

2.1. Film preparation

The ZrN/TiNiN nano-multilayer films are deposited on silicon substrates by using DC and RF magnetron co-sputtering methods (JGP-450). During the deposition, the DC power controls the Zr target (99.99% purity and 75 mm target diameter) and the RF power controls the Ti-Ni target. The Ti-Ni target is a composite target, which is made by cutting 25 equal parts of Ti target and Ni target, respectively, and assembling them by combination. In this work, the volume ratios of Ni and Ti targets are 0:25, 1:24, 2:23, 3:22, 4:21, 5:20 and 6:19, as shown in Fig. 1 with Ni:Ti = 6:19 as an example. Prior to the deposition, the silicon substrates are ultrasonically cleaned with acetone and anhydrous ethanol for 15 min, respectively, and then dried and loaded at the workpiece table in the vacuum chamber. Before the nano-multilayer films deposition, the substrates are firstly cleaned by Ar⁺ plasma sputtering for 10 min. When the vacuum pressure of the chamber is below $3\times 10^{-3}\mbox{ Pa},$ the deposition of ZrN/TiNiN nano-multilayer films begins, and the detailed sputtering parameters are as follows. The power of the Zr target is set to 180 W, while the power of the Ti-Ni composite target is 100 W. The distance between the target and the silicon substrates is 50 mm. The sputtering gas is a mixture of Ar (99.999%) and N₂ (99.999%), where the flow rate of Ar and N2 is controlled at 35 and 6 sccm, respectively. And the sputtering pressure is 0.5 Pa. During the deposition, a computer program

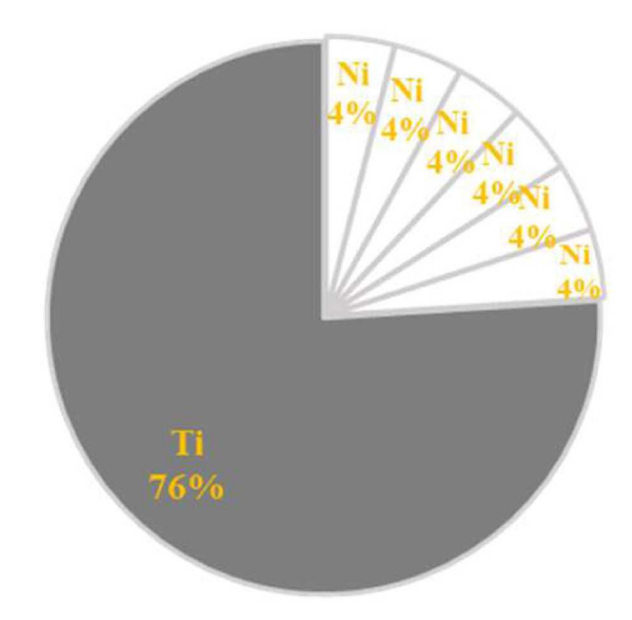


Fig. 1. The schematic picture of Ti-Ni composite target (taking Ni: ${\rm Ti}=6:19$ as an example).

is used to automatically control the rotation speed of the workpiece table to adjust the position of silicon substrate, so that the residence time of silicon substrate under the Zr target and Ti-Ni target was 15 and 5 s, respectively. Finally, a series of ZrN/TiNiN nano-multilayer films with different Ni contents were prepared with the duration period of 150 times.

2.2. Film characterizations

The phase analysis of the ZrN/TiNiN nano-multilayer films are carried out using a D8 Advance X-ray diffractometer (XRD) with a scanning range of 10° to 80° . The microstructure of ZrN/TiNiN nano-multilayer films are observed by SEM (Quanta FEG450) and HRTEM (Tecnai G2 F30). The chemical composition were analyzed by the electron probe microanalyzer (EPMA, JXA-8530 F PLUS) with accelerating voltage 15 kV, current 20 nA, and beam spot 1 μ m/min. The FST1000 film stress tester is used to test the internal stress in the films by measuring the curvature radius of the silicon wafer before and after coating. The thickness of the silicon substrate is about 0.5 mm with the size of 5 mm \times 10 mm. The thicknesses of the nano-multilayer films are 1–2 μ m. And then the internal stress is calculated using Stoney's formula. The hardness, elastic modulus and fracture toughness of the films are tested using a TI 980 nano-indenter. The depth of indentation is accurately recorded as a function of load. The hardness and elastic modulus of the nano-multilayer films are calculated using the Oliver-Pharr model [38]. Here, the indentation depth is set at 100 nm, which is less than 1/10 of the thickness of the nano-multilayer films, so as to eliminate the influence of the substrate on the hardness of the films. The six different indentation locations are measured for each sample to confirm the reliability of the data. For fracture toughness measurement, the indentation depth is set at 80% of the film thickness. The fracture toughness (K_{IC}) is calculated as shown in Eq. (1) [39-42].

$$K_{IC} = \alpha \left(\frac{E}{H}\right)^{\frac{1}{2}} \left(\frac{P}{C_2^{\frac{1}{2}}}\right) \tag{1}$$

where α is a constant related to the indenter geometry, depending on the indenter geometry, Berkovich indenters take 0.0016. E and H are the elastic modulus and hardness of the measured material, respectively. P is the indentation load. And C is the crack length.

3. Results

3.1. Effect of Ni content on the microstructures of ZrN/TiNiN nano-multilayer films

Fig. 2 shows the variation of element contents in ZrN/TiNiN nanomultilayer films. Considering the difference in the sputtering rates of Ni and Ti targets, the element contents present different in the asdeposited nano-multilayers. The results showed that when the volume ratios of Ni and Ti in the Ti-Ni composite target are 0:25, 1:24, 2:23, 3:22, 4:21, 5:20 and 6:19, respectively, the Ni contents in ZrN/TiNiN nano-multilayer films were 0, 2.39 at%, 3.83 at%, 5.81 at%, 6.98 at%, 7.77 at% and 9.38 at%, respectively. Whereas, the Ti contents were 3.51 at%, 3.28 at%, 2.05 at%, 1.48 at%, 1.35 at%, 1.14 at% and 0.05 at %, respectively. It indicated that with the increase of the volume ratio of Ni and Ti in the Ti-Ni composite target, the Ni content in the film gradually increased, while the Ti content gradually decreased. Besides, the Zr and N contents were also influenced by the volume ratio of Ni and Ti in the Ti-Ni composite target. When Ni:Ti volume ratio in the Ti-Ni composite target increased, the Zr content decreased, yet N content slightly increased. Therein, the decrease of Zr content is attributed to the both increases of Ni content and N content. Besides, because Ni atom hardly reacts with N atom, the N atom or N2 would adsorb physically on the Ti-Ni target. With Ni:Ti volume ratio increasing, the more N atoms would be adsorbed on the Ti-Ni target, thus leading to that more N atoms were sputtered and deposited in the ZrN/TiNiN nano-multilayer films. In addition, the N content was lower than 50 at%, which is mainly due to the fact that the metal Ni does not react easily with the N atom. Compared with Zr and Ti, the chemical activity of Ni is lower, which is relatively difficult to form compounds with N atom. Therefore, from the point of view of reaction thermodynamics, ZrN or TiN is easier to form than NiN. Moreover, the formation of ZrN and TiN will be preferred due to those free energies of formation being much lower.

Fig. 3 presents the XRD patterns of ZrN/TiN and ZrN/TiNiN nanomultilayer films with different Ni contents. When Ni content is zero at Ni:Ti= 0:25, the XRD spectrum for the ZrN/TiN nano-multilayer film only present ZrN (111) diffraction peak at 2θ = 33.93°. When the Ni atoms were introduced in the ZrN/TiNiN nano-multilayer films, the three diffraction peaks in the XRD spectra appeared at 2θ = 33.93°, 39.33° and 56.79°, which corresponded to FCC ZrN (111), (200) and (220) crystal planes, respectively [33,34]. In this case, all nano-multilayer films showed a distinct ZrN (111) diffraction peak at 2θ = 33.93°, which indicated that they had the same preferred growth orientation. Besides, when Ni:Ti = 1:24, the intensity of ZrN (111)

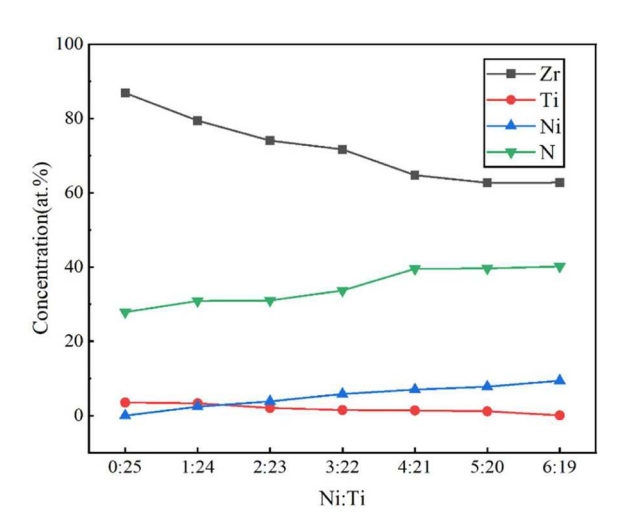


Fig. 2. Variation of element contents in the ZrN/TiN and ZrN/TiNiN nanomultilayer films.

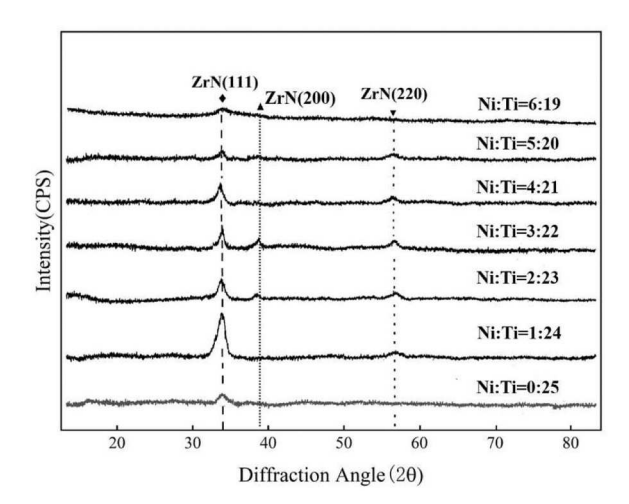


Fig. 3. XRD patterns of the ZrN/TiN and ZrN/TiNiN nano-multilayer films with different Ni contents.

diffraction peak for the ZrN/TiNiN nano-multilayer film increased obviously compared with that of the ZrN/TiN nano-multilayer film. Wherein, the intensity of the ZrN (111) diffraction peak was highest when Ni:Ti = 1:24, indicating the best crystallinity of the ZrN/TiNiN nano-multilayer film. In addition, with Ni content increasing, the intensity of ZrN (111) diffraction peak gradually decreased. Moreover, it is found that there is no XRD peak of TiN or Ni in the XRD pattern. The reasons are as follows. Firstly, it was mainly due to that it is very close to the diffraction angle of TiN and ZrN at (111) and (220) of FCC structure. Secondly, the thickness of modulation layer is very thin with fewer TiN and Ni phase.

Fig. 4 shows the cross-section HRTEM images of the ZrN/TiNiN nano-multilayer films at Ni:Ti= 1:24. In the Fig. 4(a) with a low magnification HRTEM image, it showed that the film had a clear periodic multilayer structure with a distinct contrast difference between the layers. Fig. 4(b) was a further enlarged image based on the Fig. 4(a). Therein, the light stripes were the ZrN layers and the dark stripes were the TiNiN layers, of which the thicknesses were 11.2 ± 0.5 and 4.3 \pm 0.3 nm, respectively. At the lower right-hand corner in the Fig. 4(b), it was a magnified image of the area marked by red box A at the interface of the main layer (ZrN) and the modulation layer (TiNiN). At this time, it was observed that the lattice stripe crossed the interface, allowing the nano-multilayer films to remain continuous within the main layer and the modulation layer, which indicated that the TiNiN layer was coherent epitaxial grown by the "template effect" [43,44] under the ZrN layer. Meanwhile, the TiN and Ni interface phases in the modulation layer appeared in a crystalline state. In the Fig. 4(c), the spacing of crystalline surface d of (111) plane was about 0.275 nm. When Ni:Ti= 1:24, the interfacial phase present crystallization, which might be resulted from that the TiNiN modulation layer and the main ZrN layer maintained coherent epitaxial growth. In the Fig. 4(d) of the selected electron diffraction pattern, the (111), (200), and (311) crystal planes were marked according to the plane spacing d, which were consistent with the XRD results. After calculation, the crystal zone axis corresponding to the diffraction spots was [01-1], which indicated that FCC structure was displayed in the ZrN/TiNiN nano-multilayer film at Ni:Ti= 1:24.

Fig. 5 presents the cross-section SEM images of ZrN/TiN and ZrN/TiNiN nano-multilayer films with different Ni contents. It was found that the thicknesses of all the nano-multilayer films were less than 2 μm . Also, the thickness of the ZrN/TiNiN nano-multilayer film was larger than the ZrN/TiN nano-multilayer films. It was due to the higher sputtering yield of Ni target compared with that of Ti target, which was resulted from the poor reaction between Ni and N atoms. Besides, no obvious voids appeared at the interface between the films and the substrates, indicating good adhesion of the films and the substrates.

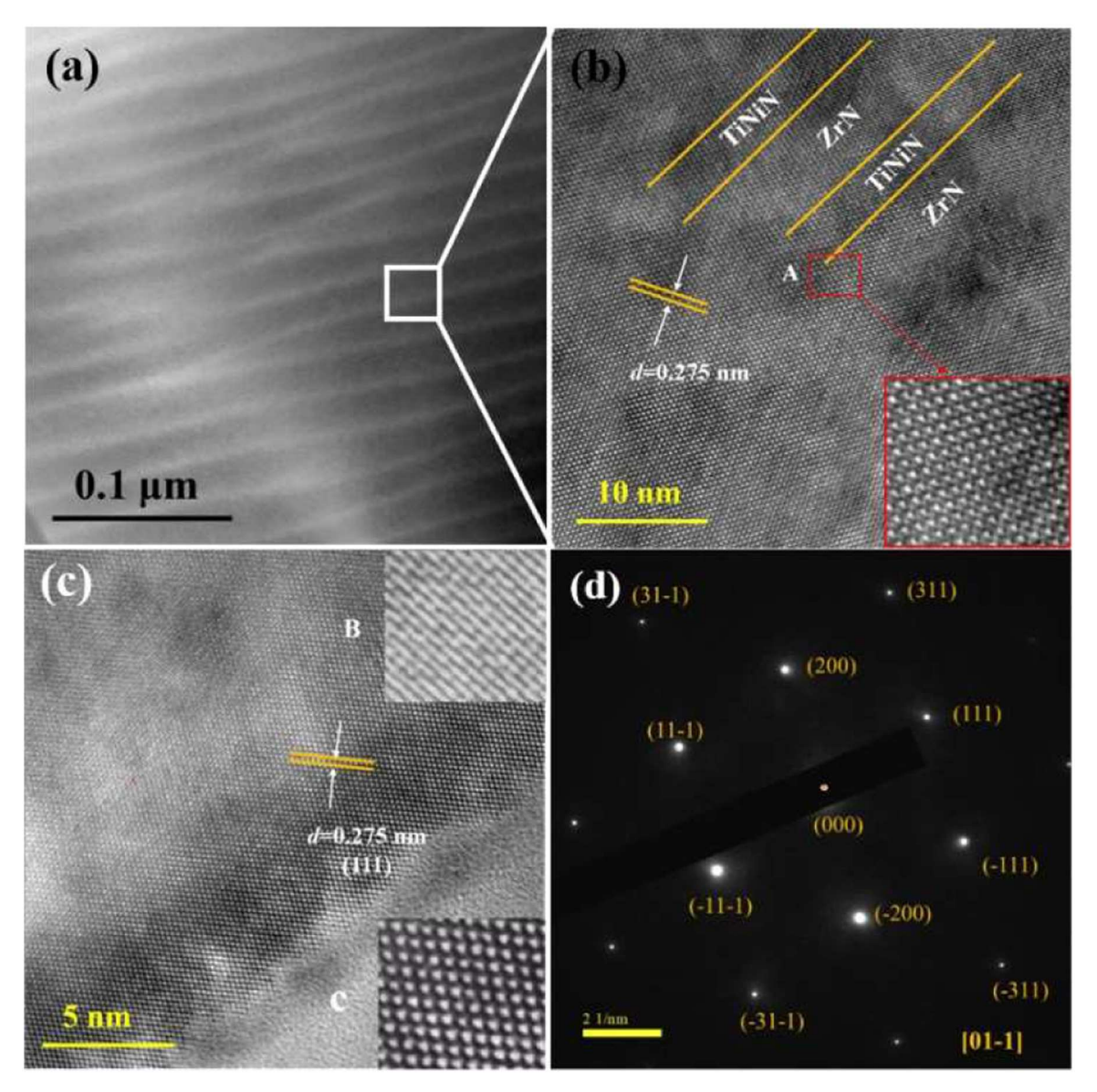


Fig. 4. Cross-section HRTEM images and selected area electron diffraction of ZrN/TiNiN nano-multilayer film at Ni:Ti= 1:24: (a) low magnification; (b) medium magnification; (c) high magnification; (d) selected area electron diffraction.

Moreover, the cross-section SEM images in the all nano-multilayer films present columnar crystal growth characteristics, except for the nano-multilayer film at Ni:Ti= 4:21, as shown in Fig. 5(e). When Ni: Ti= 1:24, columnar crystals in the ZrN/TiNiN nano-multilayer film was found throughout the film. While, with further increase in the Ni content, the columnar crystal growth became worse. It suggested that when increasing the Ni content, the columnar growth structure in the ZrN/TiNiN nano-multilayer film would be weakened and the modulation layer could not maintain coherent epitaxial growth with the main layer.

3.2. Effect of Ni content on the mechanical properties of ZrN/TiNiN nano-multilayer films

Fig. 6 shows variations of the hardness and elastic modulus for the ZrN/TiN and ZrN/TiNiN nano-multilayer films with different Ni contents. It can be seen that when no Ni was added, the hardness and elastic modulus of the ZrN/TiN nano-multilayer film was 18.8 GPa and 195.8 GPa, respectively. When Ni was introduced, the hardness and elastic modulus of the ZrN/TiNiN nano-multilayer films increased. However, with Ni content increasing, the hardness and elastic modulus

of the ZrN/TiNiN nano-multilayer films showed a trend of decreasing. When Ni:Ti = 1:24, the ZrN/TiNiN nano-multilayer film exhibited optimum hardness and elastic modulus of 23.2 GPa and 317.8 GPa, respectively.

Fig. 7 exhibits the variation of the internal stress for the ZrN/TiN and ZrN/TiNiN nano-multilayer films with different Ni contents. The internal stress was calculated through the Stoney equation [45]. It was found that the values of the internal stresses for all the nano-multilayer films were negative, which indicated that all the films were subjected to compressive stresses. When Ni content is 0, the compressive stress of the ZrN/TiN nano-multilayer film was about 0.36 GPa. However, when a small number of Ni atoms were introduced at Ni:Ti= 1:24, the compressive stresses of the ZrN/TiNiN nano-multilayer films was the smallest with a value of approximate 0. Moreover, when Ni content further increased, the compressive stresses of the ZrN/TiNiN nano-multilayer films exhibited a tendency of first increasing and then decreasing.

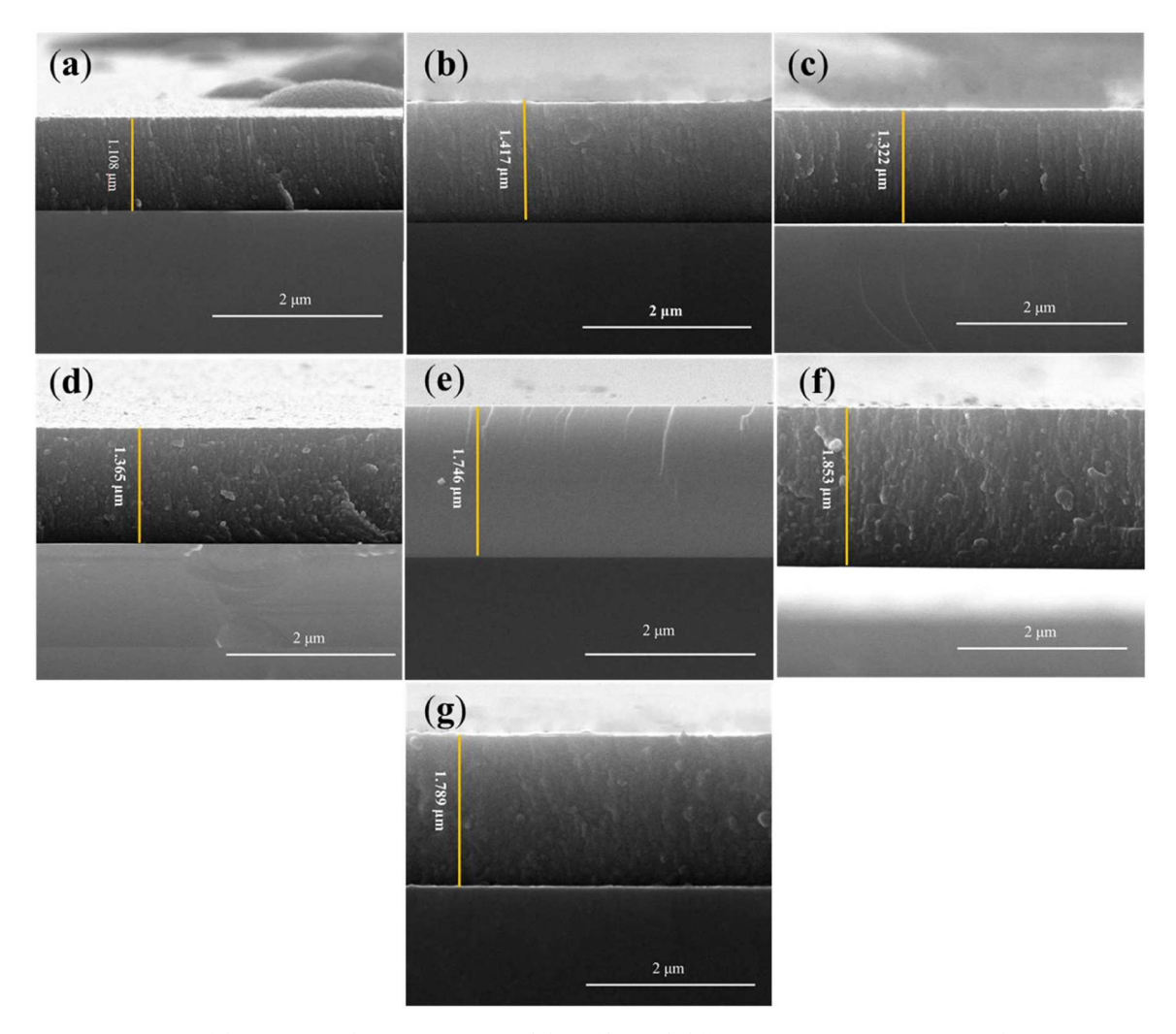


Fig. 5. Cross-section SEM images of the ZrN/TiN and ZrN/TiNiN nano-multilayer films with different Ni contents (a) Ni:Ti= 0:25; (b) Ni:Ti= 1:24; (c) Ni:Ti= 2:23; (d) Ni:Ti= 3:22; (e) Ni:Ti= 4:21; (f) Ni:Ti= 5:20; (g) Ni:Ti= 6:19.

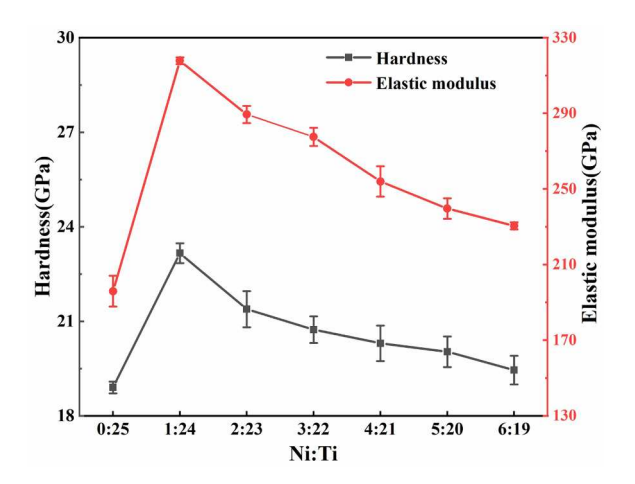


Fig. 6. Variations of hardness and elastic modulus of the ZrN/TiN and ZrN/TiNiN nano-multilayer films with different Ni contents.

3.3. Effect of Ni content on the fracture toughness of ZrN/TiNiN nanomultilayer films

Fig. 8 shows the SEM images of indentations on the ZrN/TiN and ZrN/TiNiN nano-multilayer films with different Ni contents. In this

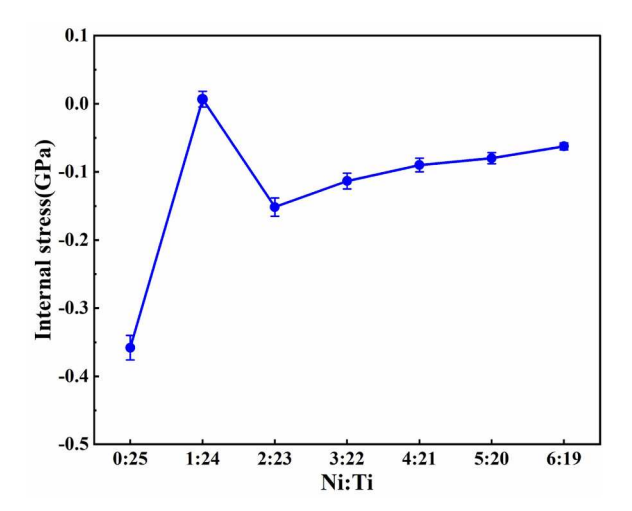


Fig. 7. Variation of internal stress in the ZrN/TiN and ZrN/TiNiN nanomultilayer films with different Ni contents.

experiment, the indentation tests were carried out using the Berkovich indenter, and the depth of indentation was chosen to be 80% of the film thickness, approximately 1500 nm, in order to further evaluate the fracture toughness ($K_{\rm IC}$) of the nano-multilayer films. It was found that

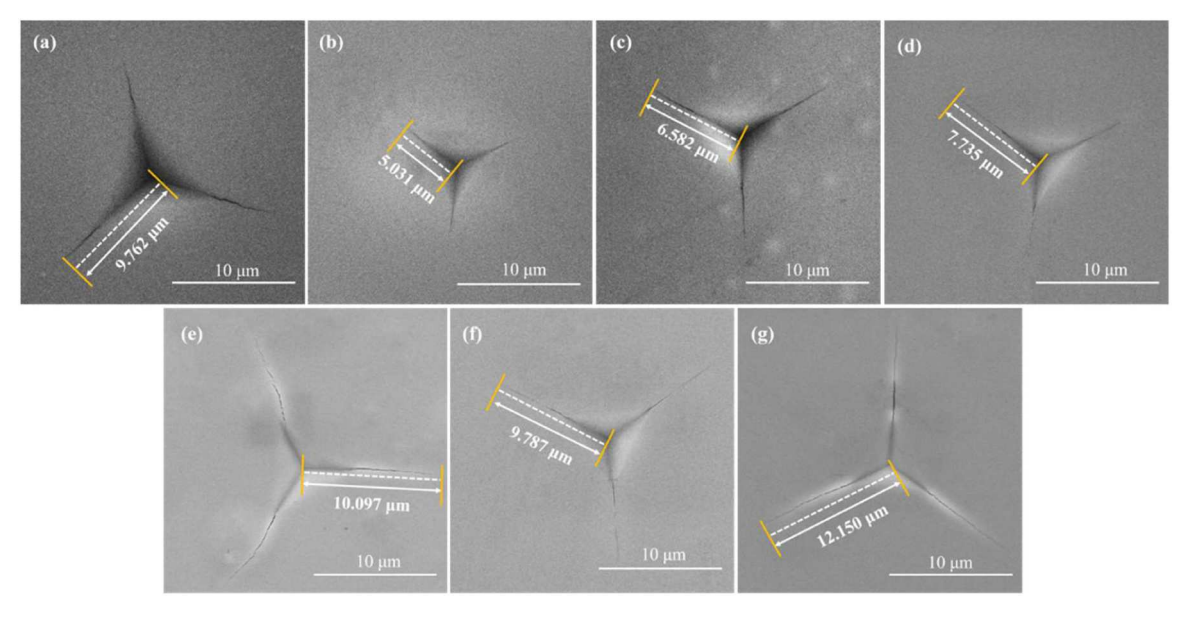


Fig. 8. SEM images of indentations on the surfaces of ZrN/TiN and ZrN/TiNiN nano-multilayer films at an indentation depth of 1500 nm. (a) Ni:Ti= 0:25; (b) Ni: Ti= 1:24; (c) Ni:Ti= 2:23; (d) Ni:Ti= 3:22; (e)Ni:Ti= 4:21; (f) Ni:Ti= 5:20; (g) Ni:Ti= 6:19.

the surfaces of the as-deposited nano-multilayer films showed obvious radial cracks and extrusion cracks formed by indenter squeezing. For the ZrN/TiN nano-multilayer film, the crack length was 9.762 μm . When Ni: Ti =1:24 (Fig. 8b), the shortest radial crack length with the value of 5.031 μm was observed on the surface of the ZrN/TiNiN nano-multilayer film, indicating that the film exhibited the best fracture toughness. As Ni content increased, the radial crack length gradually increased.

According to the toughness calculation Eq. (1), the calculated values of K_{IC} are shown in Fig. 9. It present that the fracture toughness K_{IC} values of all the ZrN/TiNiN nano-multilayer film were larger than that of the ZrN/TiN nano-multilayer film. Besides, the fracture toughness K_{IC} values of the ZrN/TiNiN nano-multilayer films showed a trend of decreasing as the Ni content increased. The maximum fracture toughness K_{IC} values of the nano-multilayer films was achieved at Ni:Ti= 1:24, with a value of 2.29 MPa \bullet m^{1/2}. It suggested that the strengthening of the films and the inhibition of crack expansion was enhanced at this Ni content, indicating that the ZrN/TiNiN nano-multilayer film exhibited the best crack resistance and that the fracture toughness of the ZrN/TiNiN nano-multilayer film was significantly improved.

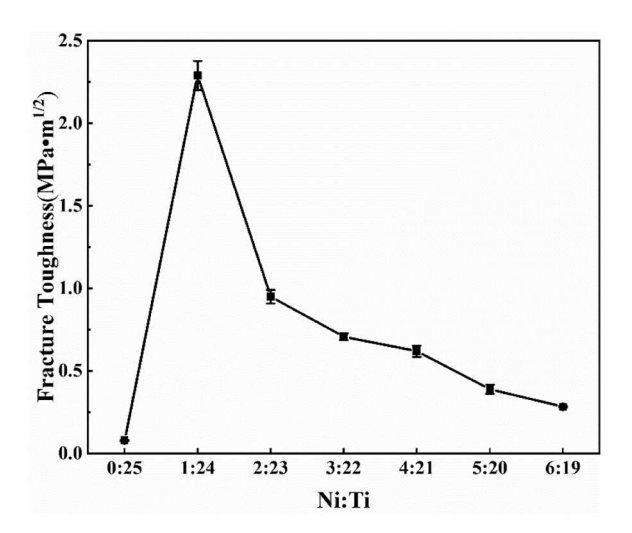


Fig. 9. Variation of fracture toughness $K_{\rm IC}$ values of ZrN/TiN and ZrN/TiNiN nano-multilayer films with different Ni contents.

4. Discussion

4.1. Microstructure evolutions in the ZrN/TiNiN nano-multilayer films

When the film grew in the atomic or molecular state on the substrate from the initial nucleation, the interface energy was the main part of the system energy, and the substrate surface had an important influence on the growth of the film. In the nano-multilayer films, the crystal structure of the firstly deposited layer can similarly have a significant effect on the crystal growth and structure of the later deposited layer. Therefore, the subsequently deposited layer formed a crystal structure that had a good interface match with the first deposited layer, which was called the "template effect". This phenomenon occurred in the previous studies on the nano-multilayer films, such as TiN/NbN [46], TiN/VN [47], CrN/AlN [48], TaN/AlN [49], etc. In the ZrN/TiNiN nano-multilayer films, the TiNiN modulation layer formed metastable state under the action of the ZrN template with a stable FCC structure, resulting in the ZrN/TiNiN nano-multilayer films showing a FCC structure.

Combined with XRD, it can be seen that the only crystalline phase present in the nano-multilayer films was ZrN, which was independent of the Ti and Ni elements. It suggested that the Ti and Ni in the modulation layer might be dissolved within the crystalline ZrN phase or separated during the deposition process to form an amorphous phase rich in TiN and Ni. This phenomenon was consistent with previous studies in the literatures, such as the absence of modulation layer diffraction peaks in the XRD peaks of CrN/TiSiN [50] and TiN/Ni [51] films. In addition, the (111) diffraction peaks of the ZrN/TiNiN nano-multilayer films were shifted to the right as a whole. The shift in the diffraction peaks was due to the difference in the lattice constants of the nano-multilayer films when the ZrN and TiNiN layers were grown alternately, resulting in tensile/stress growth at the interface between the two layers. The lattice parameters of ZrN and TiN were 0.459 nm and 0.424 nm, respectively. For the purpose of coherent epitaxial growth at the interface, the ZrN main layer sustained compressive stress, resulting in the decrease of lattice constant, while the tensile stress of TiNiN layer led to the increase of lattice constant. Therefore, in the XRD spectra, the diffraction peak of (111) crystal plane with preferred orientation shifted to the right, leading to the nano-multilayer films in a compressed state.

Based on HRTEM images, ZrN/TiNiN nano-multilayer film with Ni: Ti=1:24 exhibited a well-defined layered structure with clear interfaces and columnar structures through several modulation cycles of the nano-

multilayer film. Combined with the selected area electron diffraction pattern, it was confirmed that the ZrN/TiNiN nano-multilayer film showed FCC structure. Besides, the cross-section SEM images of the ZrN/TiNiN nano-multilayer film clearly showed the columnar crystal structure, which might be due to the coherent epitaxy growth under the "template effect" of the ZrN layer. With the Ni content increasing, the number of Ni amorphous phases increased, giving the TiNiN layer an amorphous character. Therein, the epitaxial growth structure would be destructed, and thus the columnar growth is weakened.

In conclusion, the microstructure evolution of ZrN/TiNiN nanomultilayer films was displayed in the Fig. 10. When Ni:Ti= 1:24, the intensity of the(111) diffraction peak of ZrN was the strongest. Due to the relatively low Ni content, Ni atoms might be dissolved in TiN to form TiNiN solid solution together. Similar result was reported for fcc-(Ti, Al) N in the earlier work [33]. Besides, the TiNiN modulation layer was grown by coherent epitaxy under the "template effect" of the ZrN layer, as shown in Fig. 10 (a). When the Ni content was further increased, the number of TiN crystalline phases in the modulated layer decreased and the number of Ni amorphous phases increased. Therein, the TiN crystals with different dislocations were distributed in the amorphous Ni phase, giving the TiNiN layer an amorphous character. In this case, the ZrN layer hardly maintain the "template effect" on the TiNiN layer, resulting in the destruction of the epitaxial growth structure, as shown in Fig. 10 (b).

4.2. Improvement of hardness and fracture toughness in the ZrN/TiNiN nano-multilayer films

Hardness, elastic modulus and residual stresses are closely related to the microstructures of the ZrN/TiNiN nano-multilayer films. Compared to ZrN/TiN nano-multilayer films when Ni:Ti= 0:25, the hardness and elastic modulus ZrN/TiNiN nano-multilayer films were all improved, while the compressive stresses obviously decreased. It was resulted from the formation of TiNiN solid solution and coherent interface when Ni introducing. With Ni content increasing, the hardness and elastic modulus of the ZrN/TiNiN nano-multilayer films showed a decreasing trend, yet an increasing trend for the compressive stress. When Ni:Ti = 1:24, the TiNiN layer grew coherent well with the adjacent ZrN main layer. According to the modulus difference strengthening theory proposed by Koehler [52], when dislocations crossed the coherent interface, they would be hindered by stresses generated by thin film materials with different shear modulus. The greater the difference in shear modulus between the two materials, the more significantly the additional stresses

block the dislocation movement, thus the more significant the strengthening effect. Besides, the lattice parameters of ZrN and TiN are 0.459 nm and 0.424 nm, respectively. Therein, the lattice distortion would occur in the ZrN/TiNiN nano-multilayer films under epitaxial growth structure due to the Ni atoms substituting the Ti atoms in the TiNiN lattice. According to the alternating stress field theory [53], the interface would hinder the movement of dislocations and strengthened the film. Thus, modulus difference strengthening theory and alternating stress field theory combined to promote the enhancement in hardness of the ZrN/TiNiN nano-multilayer films.

The increase in fracture toughness of the ZrN/TiNiN nano-multilayer films in contrast to ZrN/TiN nano-multilayer films was mainly determined by microstructure and other factors [54]. Firstly, the beneficial ductile properties of Ni metal in modulation layers would contribute to the fracture toughness of the nano-multilayered films. When Ni:Ti = 1:24, the TiN-Ni in the modulation layer tended to maintain the coherent epitaxial growth with the ZrN layer. Therefore, the ZrN/TiNiN nano-multilayer film with Ni:Ti = 1:24 exhibited a better strengthening and toughening effect. With the further increase of Ni content, the modulation layer TiNiN changed to amorphous state, which destroyed the coherent interface between the main layer and the modulation layer, thus weakening the columnar crystal growth of the film. Without the barrier of coherent interface to dislocation movement, the strengthening effect of ZrN/TiNiN nano-multilayer films disappeared, resulting in the rapid decline of fracture toughness of the nano-multilayer films.

Based on the above discussions, the fracture toughness of ZrN/TiNiN nano-multilayer films should be assessed in terms of the film's resistance to cracking. It can be summarized as follows. Firstly, the films were more prone to radial cracking when the TiN-Ni in the modulated layer was amorphous than that when the TiN-Ni was crystalline. Secondly, when Ni: Ti = 1:24, the crack resistance effect of coherent interface was more obvious than that of non-coherent interface. Finally, the release of residual compressive stresses helped to hinder the sprouting and extension of radial cracks, as shown by the shortest radial crack length in Fig. 8, thus improving the fracture toughness of the nano-multilayer film. This suggested that when the right amount of Ni was added, the modulation layer was transformed into a crystalline state under the "template effect" of the ZrN layer. In this case, the formation of coherent structure at the interface and the release of residual compressive stress in the ZrN/TiNiN nano-multilayer film would prevent the film from crack expansion and ultimately improved the fracture toughness of the film.

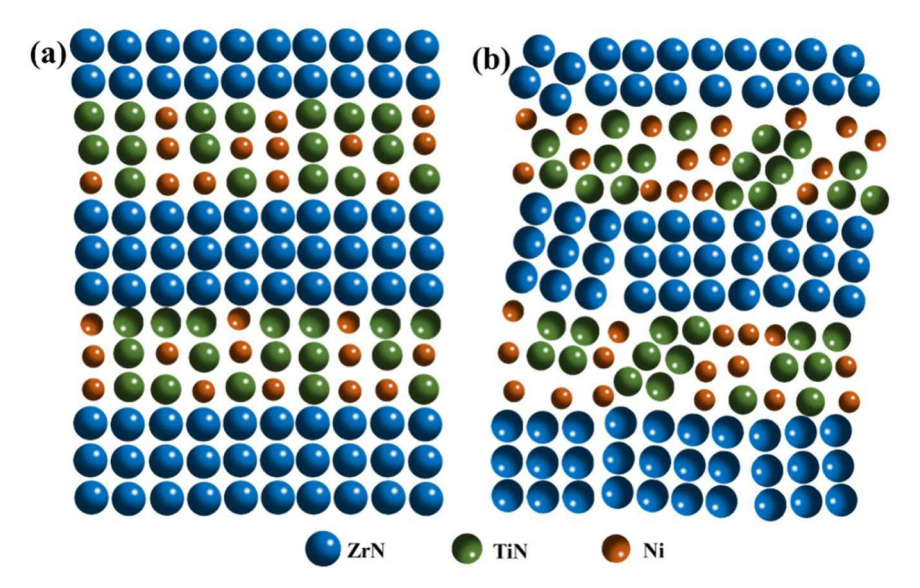


Fig. 10. Microstructure evolution of ZrN/TiNiN nano-multilayer films: (a) Ni:Ti=1:24, (b) Ni:Ti>1:21.

5. Conclusion

A series of ZrN/TiNiN nano-multilayer films with different Ni contents were successfully prepared by varying the Ni:Ti volume ratio of the targets using magnetron sputtering technique. The microstructures, mechanical properties, and fracture toughness were systematically studied. The detailed results were as follows.

- (1) The ZrN/TiNiN nano-multilayer films consisted of FCC ZrN crystalline phase with a preferred growth orientation of (111). The crystallinity of the films showed a trend of first increasing and then decreasing with increasing Ni content. When Ni:Ti = 1:24, the film exhibited the best crystalline and the film grew in columnar crystals.
- (2) When Ni was added, the hardness of the hardness and elastic modulus of the ZrN/TiNiN nano-multilayer films were all improved compared to that of the ZrN/TiN nano-multilayer films. With the increase of Ni content, the hardness and elastic modulus of the ZrN/TiNiN nano-multilayer films decreased. When Ni:Ti = 1:24, the films exhibited the maximum hardness and elastic modulus of 23.2 GPa and 317.8 GPa, respectively. It was mainly attributed to the formation of coherent interface between the ZrN layer and TiNiN layer under the combined effect of modulus difference strengthening theory and alternating stress field theory.
- (3) The ZrN/TiN and ZrN/TiNiN nano-multilayer films were all compressively stressed. However, when Ni was added, the compressive stress of the ZrN/TiNiN nano-multilayer films obviously decreased compared to that of the ZrN/TiN nanomultilayer films. With the increase of Ni content, the compressive stresses of ZrN/TiNiN nano-multilayer films first increased and then decreased. When Ni:Ti = 1:24, the internal stress was minimized, approaching to 0. At this time, the fracture toughness of the films also reached the maximum value of 2.29 MPa·m $^{1/2}$, showing the best resistance to crack extension. It indicated that when an appropriate amount of Ni was added in the ZrN/TiNiN nano-multilayer film, the TiNiN modulation layer changed to crystalline state, and the coherent structure was formed at the interface. Therein, combined with the release of residual compressive stress, they together prevented the crack propagation of the film, thus improving the fracture toughness of the ZrN/ TiNiN nano-multilayer film.

CRediT authorship contribution statement

Zhang Ke: Supervision, Investigation. Ma Fengcang: Supervision, Resources. Chen Xiaohong: Supervision, Resources. Liaw Peter K.: Writing – review & editing, Validation. Li Wei: Writing – review & editing, Supervision, Resources, Project administration, Funding acquisition. Liu Ping: Supervision, Resources, Project administration. Wang Jingjing: Writing – review & editing, Writing – original draft, Visualization, Formal analysis, Data curation. Cai Yingyun: Writing – original draft, Visualization, Data curation. Ma Xun: Supervision, Formal analysis.

Declaration of Competing Interest

The authors declare that they have no known competing financial interests or personal relationships that could have appeared to influence the work reported in this paper.

Data Availability

Data will be made available on request.

Acknowledgments

The present research was financially supported by the National Natural Science Foundation of China (No. 51971148), the "Dawn" Program of Shanghai Education Commission, China (No. 21SG45), the Shanghai Science and Technology Commission (22010503000) and the Shanghai Engineering Research Center of High-Performance Medical Device Materials (No. 20DZ2255500). PKL very much appreciates the supports of the Army Research Office Project (W911NF-13–1-0438 and W911NF-19–2-0049) and the National Science Foundation (DMR-1611180 and 1809640).

References

- E. Contreras, G. Bejarano, M. Gómez, Synthesis and microstructural characterization of nanoscale multilayer TiAlN/TaN coatings deposited by DC magnetron sputtering, Int. J. Adv. Manuf. Technol. 101 (1) (2019) 663–673.
- [2] P. Cui, W. Li, P. Liu, et al., The influence of WS₂ layer thickness on microstructures and mechanical behavior of high-entropy (AlCrTiZrNb)N/WS₂ nanomultilayered films, Surf. Coat. Technol. 433 (2022) 128091.
- [3] J.L. Qi, L.P. Wang, Y. Zhang, et al., Amorphous AlN nanolayer thickness dependent toughness, thermal stability and oxidation resistance in TaN/AlN nanomultilayer films, Surf. Coat. Technol. 405 (2021) 126724.
- [4] R. Yigit, E. Celik, F. Findik, et al., Tool life performance of multilayer hard coatings produced by HTCVD for machining of nodular cast iron, Int. J. Refract. Met. Hard Mater. 26 (6) (2008) 514–524.
- [5] H. Lind, R. Forsén, B. Alling, et al., Improving thermal stability of hard coating films via a concept of ulticomponent alloying, Appl. Phys. Lett. 99 (9) (2011) 091903.
- [6] S. Du, K. Zhang, M. Wen, et al., Crystallization of SiC and its effects on microstructure, hardness and toughness in TaC/SiC multilayer films, Ceram. Int. 44 (1) (2018) 613–621.
- [7] P. Ren, K. Zhang, M. Wen, et al., The roles of Ag layers in regulating strengthening-toughening behavior and tribochemistry of the Ag/TaC nano-multilayer films, Appl. Surf. Sci. 445 (2018) 415–423.
- [8] R. Hahn, M. Bartosik, R. Soler, et al., Superlattice effect for enhanced fracture toughness of hard coatings, Scr. Mater. 124 (2016) 67–70.
- [9] O.V. Maksakova, S. Zhanyssov, S.V. Plotnikov, et al., Microstructure and tribomechanical properties of multilayer TiZrN/TiSiN composite coatings with nanoscale architecture by cathodic-arc evaporation, J. Mater. Sci. 56 (8) (2021) 5067-5081
- [10] J. Buchinger, A. Wagner, Z. Chen, et al., Fracture toughness trends of modulus-matched TiN/(Cr,Al)N thin film superlattices, Acta Mater. 202 (2021) 376–386.
- [11] M.R. An, Q. Deng, M.J. Su, et al., Dependence of deformation mechanisms on layer spacing in multilayered Ti/Al composite, Mater. Sci. Eng. A 684 (2017) 491–499.
- [12] D. Yu, L. Yu, P. Jia, et al., Microstructure, mechanical and tribological properties of TaCN composite films by reactive magnetron sputtering, Ceram. Int. 46 (13) (2020) 20683–20694.
- [13] R.D. Arnell, P.J. Kelly, Recent advances in magnetron sputtering, Surf. Coat. Technol. 112 (1-3) (1999) 170–176.
- [14] V. Thampi, A. Bendavid, B. Subramanian, Nanostructured TiCrN thin films by pulsed magnetron sputtering for cutting tool applications, Ceram. Int. 42 (8) (2016) 9940–9948.
- [15] L. Qin, J. Wang, Q. Wu, et al., In-situ observation of crack initiation and propagation in Ti/Al composite laminates during tensile test, J. Alloy. Compd. 712 (2017) 69–75.
- [16] S. Du, K. Zhang, M. Wen, et al., Crystallization of SiC and its effects on microstructure, hardness and toughness in TaC/SiC multilayer films, Ceram. Int. 44 (1) (2017) 613–621.
- [17] S.H. Wu, Z.Q. Hou, J.Y. Zhang, et al., Understanding the strength softening of Zr/ Mo and Zr/Ti nanostructured multilayers, Scr. Mater. 172 (2019) 61–65.
- [18] A.D. Pogrebnjak, C.H. Kong, R.F. Webster, et al., Antibacterial effect of Au implantation in ductile nanocomposite multilayer (TiAlSiY) N/CrN coatings, ACS Appl. Mater. Interfaces 11 (51) (2019) 48540–48550.
- [19] P.C. Wo, P.R. Munroe, Z.T. Jiang, et al., Enhancing toughness of CrN coatings by Ni addition for safety-critical applications, Mater. Sci. Eng.: A 596 (2014) 264–274.
- [20] P. Karvankova, H.D. Mannling, C. Eggs, et al., Hard and superhard Zr-Ni-N nanocomposite films, Surf. Coat. Technol. 146 (2001) 280–285.
- [21] F. Movassagh-Alanagh, M. Mahdavi, Improving wear and corrosion resistance of AISI 304 stainless steel by a multilayered nanocomposite Ti/TiN/TiSiN coating, Surf. Interfaces 18 (2020) 100428.
- [22] T. Dasgupta, U.V. Waghmare, A.M. Umarji, Electronic signatures of ductility and brittleness, Phys. Rev. B 76 (17) (2007) 174110.
- [23] S. Zhang, D. Sun, Y. Fu, et al., Toughness measurement of thin films: a critical review, Surf. Coat. Technol. 198 (1-3) (2005) 74–84.
- [24] V. Ivashchenko, S. Veprek, A. Pogrebnjak, et al., First-principles quantum molecular dynamics study of Ti_xZr_{1-x}N (111)/SiN_y heterostructures and comparison with experimental results, Sci. Technol. Adv. Mater. 15 (2) (2014) 025007.
- [25] C. Wang, J. Han, J.M. Pureza, et al., Structure and mechanical properties of Fe_{1-x}Mn_x/TiB₂ multilayer coatings: possible role of transformation toughening, Surf. Coat. Technol. 237 (2013) 158–163.

- [26] A. Akbari, C. Templier, M.F. Beaufort, et al., Ion beam assisted deposition of TiN-Ni nanocomposite coatings, Surf. Coat. Technol. 206 (5) (2011) 972–975.
- [27] M. Irie, H. Ohara, A. Nakayama, et al., Deposition of Ni/TiN nano-composite films by cathodic arc ion-plating, Nucl. Instrum. Methods Phys. Res. Sect. B: Beam Interact. Mater. At. 121 (1-4) (1997) 133–136.
- [28] A.M. Pagon, E.D. Doyle, D.G. McCulloch, The microstructure and mechanical properties of TiNNi nanocomposite thin films, Surf. Coat. Technol. 235 (2013) 394–400.
- [29] A. Rizzo, D. Valerini, L. Capodieci, et al., Reactive bipolar pulsed dual magnetron sputtering of ZrN films: The effect of duty cycle, Appl. Surf. Sci. 427 (2018) 994–1002.
- [30] J. Du, P. Zhang, Z. Cai, et al., The influence of substrate-target orientation on the properties of ZrN films deposited by arc ion plating, Phys. Procedia 18 (2011) 181–186
- [31] J.L. Ruan, D.F. Lii, H.H. Lu, et al., Microstructural and electrical characteristics of reactively sputtered ZrNx thin films, J. Alloy. Compd. 478 (1-2) (2009) 671–675.
- [32] H.M. Tung, J.H. Huang, D.G. Tsai, et al., Hardness and residual stress in nanocrystalline ZrN films: effect of bias voltage and heat treatment, Mater. Sci. Eng.: A 500 (1-2) (2009) 104–108.
- [33] Y.O. Kravchenko, E. Coy, K. Załęski, et al., Biocompatibility and electron microscopy studies of epitaxial nanolaminate (Al0.5Ti0.5)N/ZrN coatings deposited by Arc-PVD technique, Ceram. Int. 47 (24) (2021) 34648–34656.
- [34] Y.O. Kravchenko, E. Coy, B. Peplińska, et al., Micro-mechanical investigation of (Al50Ti50) N coatings enhanced by ZrN layers in the nanolaminate architecture, Appl. Surf. Sci. 534 (2020) 147573.
- [35] K. Yalamanchili, I.C. Schramm, E. Jiménez-Piqué, et al., Tuning hardness and fracture resistance of ZrN/Zr_{0.63}Al_{0.37}N nanoscale multilayers by stress-induced transformation toughening, Acta Mater. 89 (2015) 22–31.
- [36] A.D. Pogrebnjak, R.F. Webster, R.D. Tilley, et al., Formation of Si-rich interfaces by radiation-induced diffusion and microsegregation in CrN/ZrN nanolayer coating, ACS Appl. Mater. Interfaces 13 (14) (2021) 16928–16938.
- [37] O.V. Maksakova, R.F. Webster, R.D. Tilley, et al., Nanoscale architecture of (CrN/ZrN)/(Cr/Zr) nanocomposite coatings: microstructure, composition, mechanical properties and first-principles calculations, J. Alloy. Compd. 831 (2020) 154808.
- [38] W.C. Oliver, G.M. Pharr, An improved technique for determining hardness and elastic modulus using load and displacement sensing indentation experiments, J. Mater. Res. 7 (6) (1992) 1564–1583.
- [39] A.G. EVans, E.A. Charles, Fracture toughness determinations by indentation, J. Am. Ceram. Soc. 59 (7-8) (1976) 371–372.

- [40] S. Zhang, X. Zhang, Toughness evaluation of hard coatings and thin films, Thin Solid Films 520 (7) (2012) 2375–2389.
- [41] S. Zhang, D. Sun, Y. Fu, et al., Toughness measurement of thin films: a critical review, Surf. Coat. Technol. 198 (1-3) (2005) 74–84.
- [42] S. Zhang, X. Zhang, Toughness evaluation of hard coatings and thin films, Thin Solid Films 520 (7) (2012) 2375–2389.
- [43] H. Yan, Q. Tian, D. Gao, et al., Microstructure and properties of TiAlN/AlN multilayers with different modulation periods, Surf. Coat. Technol. 363 (2019) 61–65.
- [44] W. Li, P. Liu, J. Meng, et al., Microstructure and mechanical property of TiSiN nanocomposite film with inserted CrAlN nanomultilayers, Surf. Coat. Technol. 286 (2016) 313–318.
- [45] N. Koutná, L. Löfler, D. Holec, et al., Atomistic mechanisms underlying plasticity and crack growth in ceramics: a case study of AIN/TiN superlattices, Acta Mater. 229 (2022) 117809.
- [46] X. Chu, M.S. Wong, W.D. Sproul, et al., Deposition and properties of polycrystalline TiN/NbN superlattice coatings, J. Vac. Sci. Technol. A: Vac., Surf., Films 10 (4) (1992) 1604–1609.
- [47] U. Helmersson, S. Todorova, S.A. Barnett, et al., Growth of single-crystal TiN/VN strained-layer superlattices with extremely high mechanical hardness, J. Appl. Phys. 62 (2) (1987) 481–484.
- [48] M. Schlögl, J. Paulitsch, P.H. Mayrhofer, Thermal stability of CrN/AlN superlattice coatings, Surf. Coat. Technol. 240 (2014) 250–254.
- [49] J. Shuai, X. Zuo, Z. Wang, et al., Comparative study on crack resistance of TiAlN monolithic and Ti/TiAlN multilayer coatings, Ceram. Int. 46 (5) (2020) 6672–6681
- [50] W. Li, P. Liu, X. Zhu, et al., Si content dependent microstructure and mechanical properties of CrN/TiSiN nanomultilayered films, Mater. Sci. Eng.: A 610 (2014) 28–32.
- [51] I. Lopez-Cabanas, J. Llorca, R. González-Arrabal, et al., High throughput optimization of hard and tough TiN/Ni nanocomposite coatings by reactive magnetron sputter deposition, Surf. Coat. Technol. 418 (2021) 127226.
- [52] J.S. Koehler, Attempt to design a strong solid, Phys. Rev. B 2 (2) (1970) 547-551.
- [53] M. Kato, T. Mori, L.H. Schwartz, Hardening by spinodal modulated structure, Acta Metall. 28 (3) (1980) 285–290.
- [54] Q. Wang, F. Zhou, J. Yan, Evaluating mechanical properties and crack resistance of CrN, CrTiN, CrAlN and CrTiAlN coatings by nanoindentation and scratch tests, Surf. Coat. Technol. 285 (2016) 203–213.